Electron-impact-ionization cross sections for excited states of B^{q+} ($q = 0$–2) and an investigation into n scaling of ionization cross sections

Teck-Ghee Lee, S. D. Loch, C. P. Ballance, J. A. Ludlow, and M. S. Pindzola
Department of Physics, Auburn University, Auburn, Alabama 36849, USA
(Received 7 May 2010; published 29 October 2010)

Nonperturbative R-matrix-with-pseudostates (RMPS) and time-dependent close-coupling (TDCC) methods are used to determine electron-impact-ionization cross sections for the excited states of B, B^+, and B^{2+}. RMPS calculated cross sections are presented for the $1s^22s^23l$ and $1s^22s^24l$ configurations of B, the $1s^22s3l$ and $1s^22s4l$ configurations of B^+, and the $1s^23l$, $1s^24l$, and $1s^25l$ configurations of B^{2+}. It is shown that the TDCC-calculated cross sections for the $1s^22s^23s$ configuration of B, the $1s^22s3s$ configuration of B^+, and the $1s^23s$ configuration of B^{2+} are in reasonable agreement with the RMPS results. Furthermore, n scaling of these nonperturbative cross sections is investigated and a scheme proposed to allow for the extrapolation of electron-impact-ionization cross sections to higher n shells. Two semiempirical ionization cross-section expressions are fitted to the peak of the highest n-bundled RMPS cross sections for B, B^+, and B^{2+}. These are subsequently used for accurate evaluation of the higher n-shell ionization cross sections needed to obtain temperature- and density-dependent generalized collisional-radiative ionization coefficients for the impurity and transport modeling of magnetic fusion plasmas.

DOI: 10.1103/PhysRevA.82.042721 PACS number(s): 34.80.Dp

I. INTRODUCTION

Accurate electron-impact-ionization cross sections involving the ground and excited states of neutral atoms and low-charged atomic ions are needed for the collisional-radiative modeling of the moderately dense plasmas found in magnetic fusion energy experiments [1]. At low densities, only ionization cross sections from the ground and metastable states are needed. For moderately dense plasmas, ionization from excited states becomes important due to the increased overall frequency of electron-atom collisions. For highly dense plasmas, the isolated atom ground- and excited-state ionization cross sections need to be recalculated since background electrons now also screen the projectile electron from the target [2]. Along an isonuclear sequence the neutral atom and low-charged atomic ions are most sensitive to excited-state ionization since the collision frequency for these ions can easily become higher than the radiative decay frequencies. Generally, for light elements of charge $q \geqslant 3$ in moderately dense plasma environments, it is the ground- and metastable-state ionization cross sections that dominate the effective ionization rate coefficient; therefore, the excited-state ionization cross sections are not so important. However, for near neutral light atomic species, the effective ionization rate coefficient can often be dominated by ionization from excited states. For example, in neutral lithium at an electron density of 1×10^{14} cm^{-3}, the effective ionization rate coefficient was calculated to be about an order of magnitude larger than the ground-state ionization rate coefficient [3] only. This was confirmed experimentally by lithium experiments at the DIII-D tokamak [4]. Thus, accurate atomic data for excited-state ionization cross sections, often from very high n shells, are needed for near neutral species.

In recent decades, with the steady increase in the size of massively parallel supercomputers, a number of advanced nonperturbative close-coupling methods have been developed which are able to provide accurate electron-impact-ionization cross sections for the ground and excited states of neutral atoms and low-charged atomic ions. These include the R matrix with pseudostates (RMPS) [5,6], the convergent close-coupling (CCC) [7], the exterior complex scaling (ECS) [8], and the time-dependent close-coupling (TDCC) [9] methods. When the electron-impact-ionization cross sections calculated using the nonperturbative close-coupling methods are compared with those calculated using the perturbative distorted-wave method, two major trends are found. The first trend is that the agreement between close-coupling and distorted-wave calculations for the direct ionization cross section of the ground state along an isonuclear sequence becomes progressively better as the charge on the atomic ion increases. As the three-body interaction between the outgoing electrons and the remaining target core becomes dominated by the stronger residual target charge, a perturbative approximation becomes better. The second trend is that for a fixed atomic ion stage the agreement between close-coupling and distorted-wave calculations for the direct ionization cross section of an excited state becomes progressively worse as the principal quantum number of the excited state increases. As the ionization potential becomes smaller and the outgoing electrons interact for longer times, a perturbative approximation to the three-body interaction becomes worse. The aim of this article is to examine excited-state ionization for the first three ion stages of B, where one would expect neither a classical nor a perturbative calculation to be accurate. Nonperturbative calculations are performed to provide recommended data for the first few n shells in each ion. The n scaling of nonperturbative calculations for excited-state ionization cross sections of these ions are then studied to provide a recommended data set for the higher n shells for which nonperturbative calculations become prohibitively large.

Excited-state ionization cross-section calculations now exist for a range of light species. For the neutral H atom, the RMPS and TDCC methods [10] have been used to obtain the $1s$ ground state and the nl ($n \leqslant 4$) excited-state ionization cross sections. For the neutral He atom, the CCC method [11] has been used to determine the $1s^2$ ground state and the $1snl$ ($n \leqslant 4$) excited-state ionization cross sections. Similarly for

the He^+ ion, the CCC calculations [12,13] have been carried out for the $1s$ ground state and the nl ($n \leqslant 4$) excited-state ionization cross sections.

For B, B^+, and B^{2+}, previous nonperturbative calculations have been carried out for the ground and metastable terms. The ground-term ionization cross section for B has been investigated using the RMPS and TDCC methods [14]. The total ionization cross section for the $1s^2 2s^2 2p\,^2P$ term obtained using the 476-LS-term RMPS calculation was found to be substantially lower than the results from an earlier RMPS calculation with 60 LS terms [15]. It was shown that unlike almost all neutral atoms, significant excitation-autoionization contributions are found in the ionization cross section of the ground state of B. The ground- and metastable-term ionization cross sections for B^+ have also been calculated recently using a 414-LS term RMPS calculation and with the TDCC method [16]. It is found that both nonperturbative calculations for the ionization cross section of the $1s^2 2s^2$ ground configuration are in reasonable agreement with new crossed-beams measurements with low-ion-beam metastable content [16]. For the $1s^2 2s 2p\,^3P$ metastable term, the TDCC calculations for the $1s^2 2s 2p$ metastable configuration and the 414-LS term RMPS calculations are again in reasonable agreement with previous crossed-beams measurements with high-ion-beam metastable content [17]. The ground-term ionization cross section for B^{2+} has also been calculated with the RMPS and TDCC methods [18]. It is found that the TDCC and 55-LS term RMPS calculations for the ionization cross section of the $1s^2 2s$ ground configuration are in good agreement with crossed-beams measurements [18], previous RMPS and CCC calculations [19], and distorted-wave calculations [18].

In this article, the RMPS and TDCC methods are used to determine electron-impact-ionization cross sections for the excited states of B, B^+, and B^{2+}. Combined with previous close-coupling calculations for the ground terms of B, B^+, and B^{2+} and perturbative distorted-wave calculations for the ground and metastable terms of B^{3+} and B^{4+}, all of the fundamental ionization data will exist for the future generation of generalized collisional-radiative coefficients. The derived database of general collisional-radiative ionization coefficients as a function of both temperature and density will then be used to better understand the confinement effectiveness of coating heavy metal facing components with boron in current tokamak experiments [20]. The rest of the article is organized as follows. In Sec. II, we give a brief review of the RMPS, TDCC, and exchange classical impact-parameter methods as applied to electron-impact single-ionization processes. In Sec. III, we present the results for the electron-impact ionization of the excited states of B, B^+, and B^{2+}, and in Sec. IV, we conclude with a brief summary. Unless otherwise stated, all quantities are given in atomic units.

II. THEORY

A. *R*-matrix-with-pseudostates method

In our implementation of the RMPS [6] method, which is based upon signficantly modified versions of the serial RMATRIX I programs [21], the basis used to represent the $(N+1)$-electron continuum is made orthogonal to the pseudo-orbitals using a method developed by Gorczyca and Badnell [6]. With the implementation of the method on modern supercomputer architectures [22,23], we now have the capability to calculate a comprehensive set of excited-state ionization cross sections for a particular atomic species.

R-matrix theory dictates that the configuration space describing the scattering processes is split into two regions. In the inner region, which encompasses the N-electron target, the total wave function for a given LS symmetry is expanded in basis states given by

$$\Psi_k^{N+1} = A \sum_{i,j} a_{ijk} \psi_i^{N+1} \frac{u_{ij}(r_{N+1})}{r_{N+1}} + \sum_i b_{ik} \chi_i^{N+1}, \quad (1)$$

where A is an antisymmetrization operator, ψ_i^{N+1} are channel functions obtained by coupling N-electron target states with the angular and spin functions of the scattered electron, $u_{ij}(r)$ are radial continuum basis functions, and χ_i^{N+1} are bound functions which ensure completeness of the total wave function. The coefficients a_{ijk} and b_{ik} are determined by diagonalization of the total $(N+1)$-electron Hamiltonian. The availability of massively parallel computers permits the concurrent parallel diagonalization of every Hamiltonian utilizing ScaLapack libraries [24], from which the resulting eigenvalues and eigenvectors are subsequently used in the formation of the R matrix.

In the outer region, the total wave function for a given $LS\ \Pi$ symmetry is expanded in basis states given by

$$\Psi_k^{N+1} = \sum_i \psi_i^{N+1} \frac{v_i(r_{N+1})}{r_{N+1}}. \quad (2)$$

For RMPS ionization calculations, the ionization cross section is simply derived from the sum of excitation cross sections from the excited state terms to those pseudostates lying above the respective ionization limits. Excited-state ionization cross sections require significantly more partial waves to converge than the ground-state cross section, though are only required over a reduced energy range. The strength of the RMPS method for ionization is that every excited state is calculated at the same time.

B. Time-dependent close-coupling method

The TDCC method was first applied to calculate total cross sections for the electron-impact single ionization of H [25], which is the simplest quantal three-body Coulomb breakup problem. Since then the theoretical method has been applied to calculate cross sections for electron-impact excitation and ionization of many atomic systems [9]. Briefly, the time-dependent Schrodinger equation for electron scattering from one active electron in an atom is given by

$$\frac{i\,\partial \Psi(\vec{r}_1,\vec{r}_2,t)}{\partial t} = H_{\rm system}\Psi(\vec{r}_1,\vec{r}_2,t), \quad (3)$$

where the nonrelativistic Hamiltonian for the scattering system is given by

$$H_{\rm system} = \sum_{i=1}^{2} \left(-\frac{1}{2}\nabla_i^2 - \frac{Z}{r_i} + V_{\rm HX}(r_i) \right) + \frac{1}{|\vec{r}_1 - \vec{r}_2|}, \quad (4)$$

$\vec{r}_1$ and $\vec{r}_2$ are the coordinates of the two electrons, Z is the nuclear charge, and $V_{\rm HX}$ is a Hartree with local exchange potential. Expanding the total electronic wave function in coupled spherical harmonics and substitution into the time-dependent Schrodinger equation yields a set of time-dependent close-coupled partial differential equations for each LS symmetry. The initial condition for the TDCC solution is given by a product of the active bound electron and a Gaussian radial wave packet. The LS partial cross sections are obtained by extracting the partial collision probabilities from the fully time-evolved wave functions using momentum space projections.

The target radial orbitals for B, B^+, and B^{2+} were calculated in a single configuration Hartree-Fock approximation [26]. The HX potential found in Eq. (5) was constructed using bound orbitals of the B^+ $1s^22s^2$ configuration for B ionization, bound orbitals of the B^{2+} $1s^22s$ configuration for B^+ ionization, and bound orbitals of the B^{3+} $1s^2$ configuration for B^{2+} ionization. The TDCC partial cross sections for $L = 0 \rightarrow L_{\rm max}$ were topped up using configuration-average distorted-wave partial cross sections for $L = L_{\rm max} + 1 \rightarrow 50$. At $L_{\rm max}$ the distorted-wave partial cross section was compared to the TDCC partial cross section to obtain a scaling factor. The scaled distorted-wave partial cross sections for $L = L_{\rm max} + 1 \rightarrow 50$ were then added to the TDCC partial cross sections for $L = 0 \rightarrow L_{\rm max}$ to produce final total cross sections at various incident energies.

C. Semiempirical expressions for ionization

Many semiempirical and semiclassical methods have been formulated and used over the last century for the electron-impact ionization of atoms and their ions [27]. In this article we consider two semiempirical equations. Since it has been incorporated into the Atomic Data and Analysis Structure (ADAS) collisional-radiative modeling package [1], we will use a form of the exchange classical impact parameter (ECIP) as derived by Burgess [28,29]. The ECIP method consists of a classical binary encounter approach for close collisions and an impact parameter approach for the distant collisions. For excited-state ionization, the cross section is dominated by close collisions and the impact parameter part of the ECIP calculation quickly becomes negligible. We use the ECIP method to investigate scaling of the highest n-shell data for each ion; thus, we consider just the classical part of the ECIP expression, namely,

$$\sigma_{\rm ion}(n) = F^{\rm ecip} \frac{4\pi}{I_n^2(\chi+1)} \left[\frac{1}{\chi+1} \left(\chi - \frac{\chi+1}{\chi+2} \ln(\chi+1) \right) \right], \tag{5}$$

where I_n is the ionization potential for the n shell given by

$$I_n = \frac{R(Q+1)^2}{n^2}, \tag{6}$$

where Q is the charge on the atomic ion and $R = 13.6$ eV. χ is the threshold-scaled energy of the outgoing scattered electron,

$$\chi = \frac{E - I_n}{I_n}, \tag{7}$$

while E is the energy of the incoming electron. We also consider an expression by Burgess and Vriens [27]:

$$\sigma_{\rm ion}(n) = F^{\rm bv} \frac{4\pi R^2}{E + 2I_n} \left(\frac{5}{3I_n} - \frac{1}{E} - \frac{2I_n}{3E^2} \right). \tag{8}$$

Each of these expressions gives us a means of fitting our nonperturbative ionization cross sections and extrapolating it to higher n shells. In each of these expressions we have introduced a scaling factor ($F^{\rm ecip}$ and $F^{\rm bv}$) which will be used to fit these semiempirical expressions to the nonperturbative cross sections. This can then be used to extrapolate our nonperturbative data to higher n shells.

III. NONPERTURBATIVE CLOSE-COUPLING RESULTS

A. Excited-state electron-impact ionization of B atoms

The target radial wave functions for neutral boron were generated using GASP (Graphical Autostructure Package) [30], which is a Java front end for the atomic-structure code AUTOSTRUCTURE [31]. It was also employed in the generation of radial orbitals for the B^+ and B^{2+} targets described in what follows.

The spectroscopic orbitals $1s$–$5g$ were determined within a Thomas-Fermi-Dirac-Almadi (TFDA) potential. The Thomas-Fermi scaling factor for each of the orbitals was set equal to 1.0. The representation of the higher Rydberg states and the target continuum was achieved through nonorthogonal Laguerre pseudo-orbitals that were generated for all subshells from $6s$ to $12g$. They were subsequently orthogonalized to the spectroscopic orbitals and to each other. Two R-matrix calculations were carried out. Both involved the following configurations in the close coupling calculation: $1s^22s^22p$, $1s^22s^2nl$, $1s^22s2p^2$, $1s^22s2pnl$, $1s^22p^3$, and $1s^22p^2nl$. In the first calculation we used $n = 3$–12 and $l = 0$–4, giving 144 configurations and 882 LS terms. The results for the $1s^22s^22p$

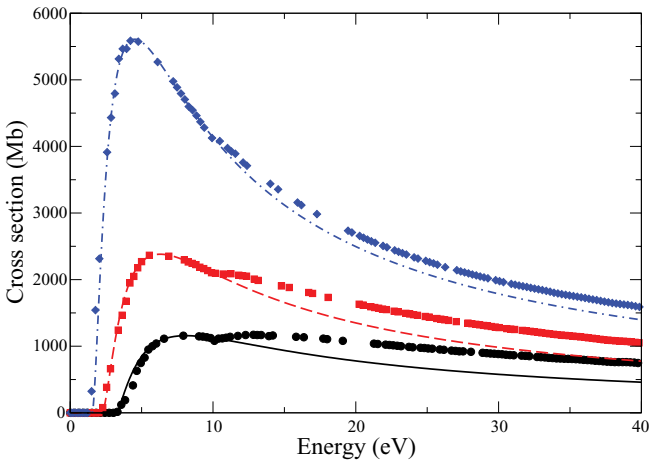

FIG. 1. (Color online) Total electron-impact-ionization cross sections for the $3l$ excited states of B. Circles, raw RMPS for $1s^22s^23s$; squares, raw RMPS for $1s^22s^23p$; diamonds, raw RMPS for $1s^22s^23d$. Solid line, fit to low-energy raw RMPS data for $1s^22s^23s$; dashed line, fit to low-energy raw RMPS data for $1s^22s^23p$; dot-dashed line, fit to low-energy raw RMPS data for $1s^22s^23d$ (1 Mb = 10^{-18} cm^2).

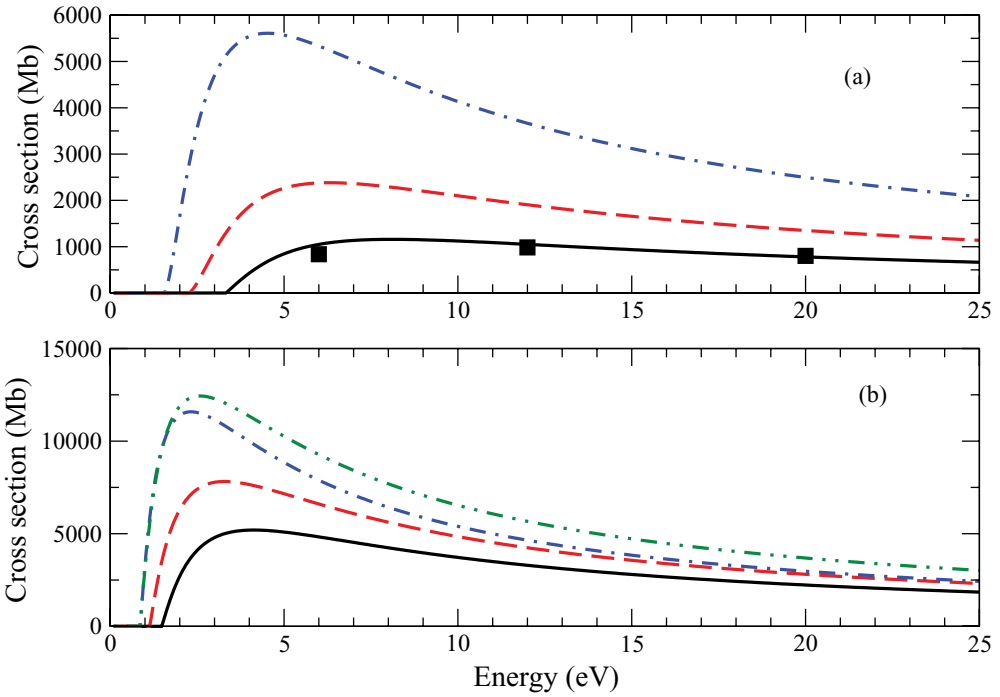

FIG. 2. (Color online) Total electron-impact-ionization cross sections for the nl excited states of B. (a) Solid line, RMPS for direct ionization of $1s^2 2s^2 3s$; dashed line, RMPS for direct ionization of $1s^2 2s^2 3p$; dot-dashed line, RMPS for direct ionization of $1s^2 2s^2 3d$. The solid squares are the TDCC results for $1s^2 2s^2 3s$. (b) Solid line, RMPS for $1s^2 2s^2 4s$; dashed line, RMPS for $1s^2 2s^2 4p$; dot-dashed line, RMPS for $1s^2 2s^2 4d$; double-dot dashed line, RMPS for $1s^2 2s^2 4f$ (1 Mb $= 10^{-18}$ cm^2).

ground state compared well with previous 476-LS-term RMPS and TDCC calculations [14]. The results for the excited states were also extracted. However, the ionization results from the $1s^2 2s^2 4f$ were not converged, requiring additional high-angular-momentum pseudostates. Thus, we performed a second calculation with the configurations listed previously, but with $n = 3$–12 and $l = 0$–5 (i.e., added in $l = 5$ to all the configurations). This calculation involved 165 configurations and 1036 LS terms. This calculation was significantly larger and therefore had to be restricted to a maximum energy of 1.1 Ry. The results agreed at lower energies with the 882-LS-term calculation for the lower nl shells, confirming that the 882-LS-term calculation had converged for those cross sections. The $1s^2 2s^2 4d$ and $1s^2 2s^2 4f$ ionization cross sections from this 1036-term calculation were used in our bundled-n and n-scaling studies. Our exchange calculation was carried out for $0 \leqslant L \leqslant 12$, a nonexchange calculation was used for $13 \leqslant L \leqslant 35$, and a "Burgess-Tully" top-up procedure [32] was used to account for higher partial waves greater than $L = 35$.

The $3s$, $3p$, and $3d$ ionization cross sections for neutral B are dominated by the direct ionization; however, excitation-autoionization of a $2s$ electron still makes a notable contribution even though the effect is much smaller than found for the ground ionization cross section. Our RMPS calculations included excitation of the $2s$ to autoionizing terms; so has the excitation-autoionization contribution included. Figure 1 shows the raw R-matrix data for the $3s$ (^2S), $3p$ (^2P), and $3d$ (^2D) terms. One can see an excitation-autoionization contribution starting around 10 eV. The rate coefficients made for neutral B use the total cross section and thus include both the direct and the indirect ionization. However, for the purposes of looking at n scaling it is more useful to consider just the direct ionization. Thus, for the $n = 3$ data we fitted just the low-energy data (below the excitation-autoionization contribution) from the $n = 3$ R-matrix calculation. This gave the solid lines shown in Fig. 1 and will be used in the n-scaling studies later in this article. The excitation-autoionization contribution for $n = 4$ appears to be negligible, as one might expect.

Figure 2 shows the data for the direct part of the $1s^2 2s^2 3l$ ($l = 0$–2) ionization cross sections (as obtained above) and the fitted data for the $1s^2 2s^2 4l$ ($l = 0$–3) cross sections. A simple analytic formula from Rost and Pattard [33] was used to fit the RMPS results and thus smooth out the few unphysical oscillations inherent in the discretization of any continuum basis.

Our TDCC calculation employed a 512×512-point radial mesh with a uniform mesh spacing of $\Delta r = 0.15$. Total cross sections for the electron-impact ionization of the $1s^2 2s^2 3s$ excited configuration are shown in Fig. 1(a). The cross section at 6 eV was topped up at $L_{\max} = 9$ with a scaling factor of 2.26, at 12 eV was topped up at $L_{\max} = 10$ with a scaling factor of 1.26, and at 20 eV was topped up at $L_{\max} = 10$ with a scaling factor of 1.14. Good agreement is found between the RMPS and TDCC results for the $3s$ ionization.

Our recommended ionization cross sections for the $n = 3$ and 4 shells of neutral boron consist of the total cross section (direct and indirect) for each of these ions. Maxwellian rate coefficients were generated from these cross sections and will be used in future generalized collisional-radiative (GCR) modeling. The cross sections for the direct ionization from the $n = 3$ shell and the data for the $n = 4$ shell are used in

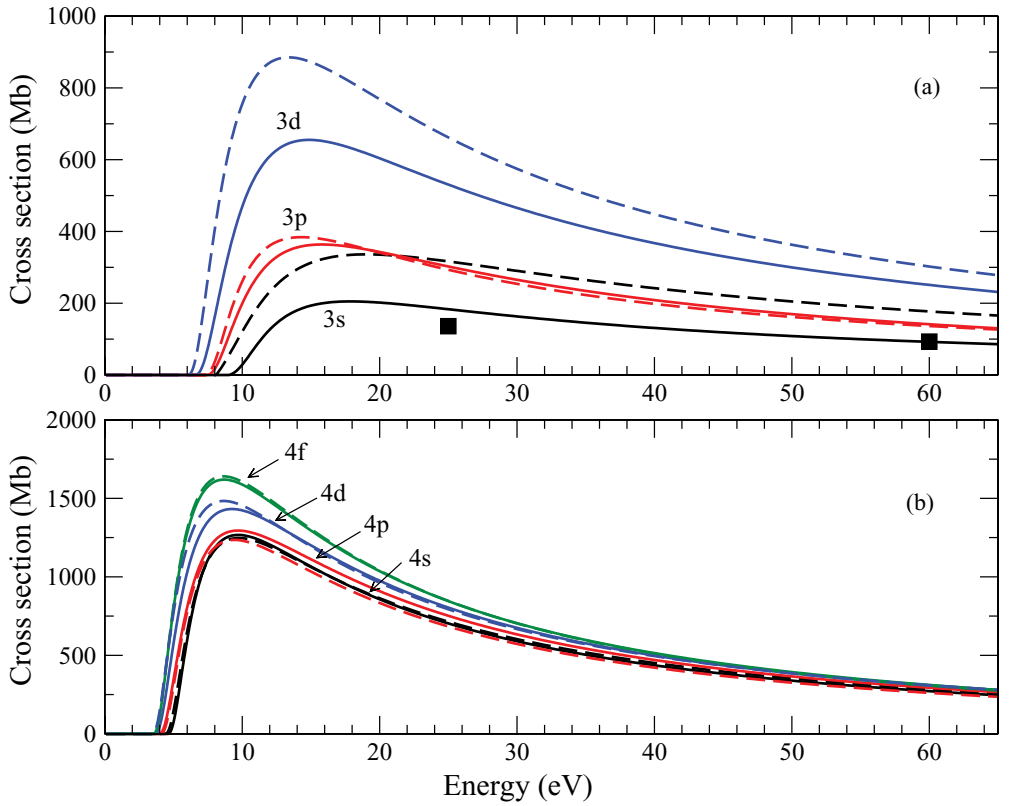

FIG. 3. (Color online) Total electron-impact-ionization cross sections for the nl excited states of B^+. (a) Black line, RMPS for $1s^2 2s 3s$; the solid black squares are the TDCC results for $1s^2 2s 3s$; and red line, RMPS for $1s^2 2s 3p$; blue line, RMPS for $1s^2 2s 3d$. (b) Black line, RMPS for $1s^2 2s 4s$; red line, RMPS for $1s^2 2s 4p$; blue line, RMPS for $1s^2 2s 4d$; green line, RMPS for $1s^2 2s 4f$. In all cases the solid line shows the results for the triplet term and the dashed line shows the results for the singlet term. The active subshells are labeled on the plots (1 Mb $= 10^{-18}$ cm^2).

Sec. III D to investigate n scaling of this RMPS data to higher n shells.

B. Excited state electron-impact ionization of B^+ ions

In the case of the B^+ ion, our RMPS calculation employed $1s$–$6h$ spectroscopic orbitals and $7s$–$14h$ Laguerre pseudo-orbitals. A total of 135 configurations, namely, $1s^2 2s^2$, $1s^2 2s 2p$, $1s^2 2snl$, $1s^2 2p^2$, and $1s^2 2pnl$ for $n = 3$–14 and $l = 0$–5, gave rise to 486 LS terms, all of which were used in the close-coupling expansion. An exchange calculation was performed for $0 \leqslant L \leqslant 14$, a nonexchange calculation was used for $15 \leqslant L \leqslant 40$, and a Burgess-Tully top-up procedure was used for the higher partial waves. The $1s^2 2s^2$ ground and $1s^2 2s 2p$ metastable cross section results compared well with previous 414-LS-term RMPS and TDCC calculations [16]. Total cross sections for the electron-impact ionization of the $1s^2 2s 3l$ ($l = 0$–2) and $1s^2 2s 4l$ ($l = 0$–3) excited configurations are shown in Fig. 3. None of the ionization cross sections showed signs of excitation-autoionization. A simple analytic formula from Rost and Pattard [33] was again used to fit the RMPS results. We note that the presence of both singlets and triplets leads to many more cross sections, with the triplet cross sections in general being lower then the singlet cross sections for the $n = 3$ data and the two spins being very close to each other for the $n = 4$ data. One exception to this is the $2s3p$ ^1P and ^3P cross sections, which have very similar ionization potentials and hence also have very similar ionization cross sections. This is as one might expect, with the electron-electron correlation effects between the $2s$ and $3p$ electrons being much smaller than the correlation between the $2s$ and $3s$ or the $2s$ and $3d$ electrons, which have a more constructive overlap of the orbital wave functions.

In our TDCC calculation, a set of radial mesh points and a mesh spacing identical to the case of neutral B were adopted. Total cross sections for the electron-impact ionization of the $1s^2 2s 3s$ excited configuration are shown in Fig. 3. The cross section at 25 eV was topped up at $L_{\max} = 9$ with a scaling factor of 0.93 and at 60 eV was topped up at $L_{\max} = 10$ with a scaling factor of 0.82. Good agreement between the RMPS and TDCC results for the $3s$ was found at 60 eV, with the TDCC results at 25 eV being lower than the RMPS results. With these RMPS cross sections we generate the Maxwellian rate coefficients and in Sec. III D we show the corresponding bundled-n cross-section data for B^+ and investigate n scaling of these cross sections.

C. Excited-state electron-impact ionization of B^{2+} ions

For the B^{2+} ion, we use $1s$–$6h$ spectroscopic orbitals and $7s$–$14h$ Laguerre pseudo-orbitals in our RMPS calculation. A total of 68 configurations, namely, $1s^2 nl$ for $n = 2$–14 and $l = 0$–5, gives rise to 68 LS terms, which were then subsequently used in the close-coupling expansion. The results for the $1s^2 2s$

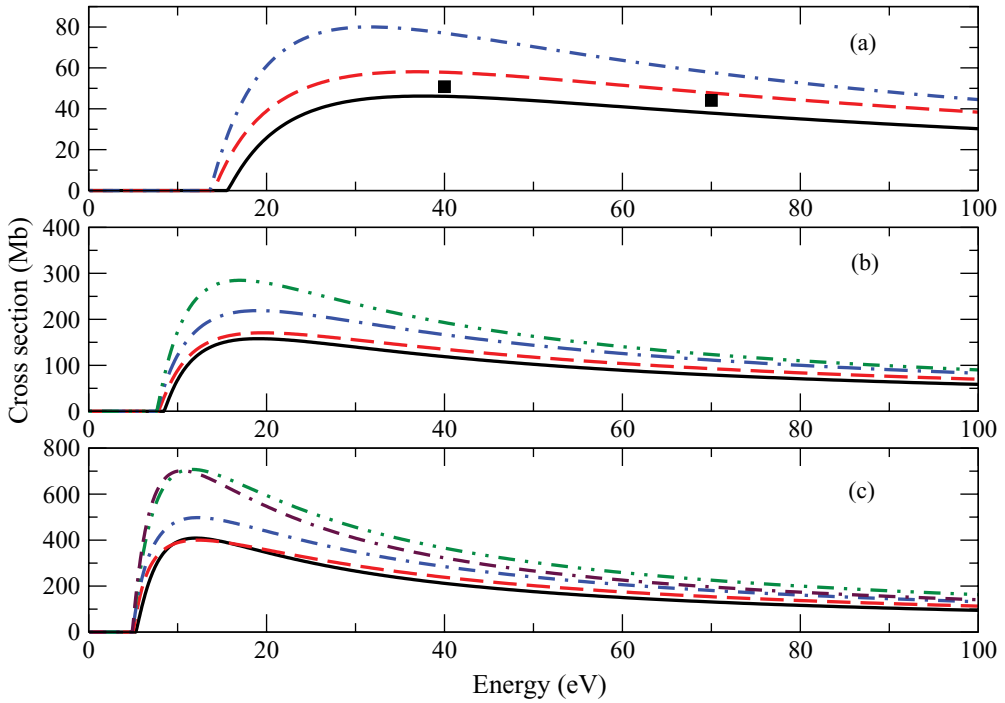

FIG. 4. (Color online) Total electron-impact-ionization cross sections for the nl excited states of B^{2+}. (a) Solid line, RMPS for $1s^2 3s\ ^2S$; dashed line, RMPS for $1s^2 3p\ ^2P$; dot-dashed line, RMPS for $1s^2 3d\ ^2D$. The solid squares show the TDCC results for the $1s^2 3s$. (b) Solid line, RMPS for $1s^2 4s\ ^2S$; dashed line, RMPS for $1s^2 4p\ ^2P$; dot-dashed line, RMPS for $1s^2 4d\ ^2D$; double-dot dashed line, RMPS for $1s^2 4f\ ^2F$. (c) Solid line, RMPS for $1s^2 5s\ ^2S$; dashed line, RMPS for $1s^2 5p\ ^2P$; dot-dashed line, RMPS for $1s^2 5d\ ^2D$; double-dot dashed line, RMPS for $1s^2 5f\ ^2F$; double-dashed dotted line, RMPS for $1s^2 5g\ ^2G$ (1 Mb $= 10^{-18}$ cm^2).

ground state are in good agreement with the previous 55-LS term RMPS and TDCC calculations [18]. An exchange calculation was carried out for partial waves with $0 \leqslant L \leqslant 12$ and a nonexchange calculation was used for $13 \leqslant L \leqslant 40$. A Burgess-Tully top-up procedure was again used to account for contributions from the higher partial waves.

Total cross sections for the electron-impact ionization of the $1s^2 3l$ ($l = 0$–2), $1s^2 4l$ ($l = 0$–3), and $1s^2 5l$ ($l = 0$–4) excited configurations are shown in Fig. 4. A simple analytic formula (from Rost and Pattard [33]) was again used to fit the RMPS results.

Similar to the preceding cases, we have kept the same set of radial mesh points and mesh spacing in our time-dependent scattering calculations. Figure 4 depicts the total cross sections for the electron-impact ionization of the $1s^2 3s$ excited configuration. The cross section at 40 eV was topped up at $L_{\max} = 9$ with a scaling factor of 1.12 and at 70 eV was topped up at $L_{\max} = 10$ with a scaling factor of 1.00. The TDCC results for the $3s$ ionization cross section are found to be in agreement with the RMPS results. Maxwellian rate coefficients were generated using the preceding cross sections and the bundled-n cross-section data for B^{2+} and the analysis of n scaling of these cross sections is shown in the following section.

D. Data for higher n shells

For generalized collisional-radiative modeling, excited-state atomic data are progressively bundled into coarser resolution as the n shell increases. For example, the ADAS codes typically consider term or level resolved data for $n \leqslant 5$ and bundled-n or bundled-nS data for the higher n shells. Bundled-n data average all of the rate coefficients within an n shell, weighted by their statistical weights. Bundled-nS also averages the data within an n shell, but built upon the spin of the parent. So, for example, in B^+ one would average the singlets within an n shell separately from the triplets. Thus, we look at bundled ionization cross sections, seeking to generate accurate ionization data for n shells above the explicitly calculated nonperturbative data. In this section we consider ways of n scaling the nonperturbative data to higher n shells. A purely classical calculation would have an n^4 scaling. Thus, while excited-state ionization cross sections for these ions are not well described by classical cross sections, one might expect the nonperturbative data to show a similar scaling to the classical results for the higher n shells. This is a similar approach to the n^3 scaling that is sometimes done on nonperturbative data for effective collision strengths that allows the low n-shell data to be extrapolated to higher n shells [34].

Figure 5 shows the n scaled results for each of our ions. That is, we show the cross section divided by n^4 versus the threshold scaled energy. The bundled-n RMPS data for B^+ and B^{2+} are well described by an n-scaled cross section. Thus, we have some confidence that scaling this data to higher n shells would result in accurate data for the more highly excited states. For neutral B, we bundle the direct cross sections that were extracted from the $n = 3$ results and compare them with the bundled-n results for $n = 4$. There are differences of about 20% at the peak of the n-scaled cross section. Thus, it appears that for neutral B, convergence onto an n^4 scaling has not yet

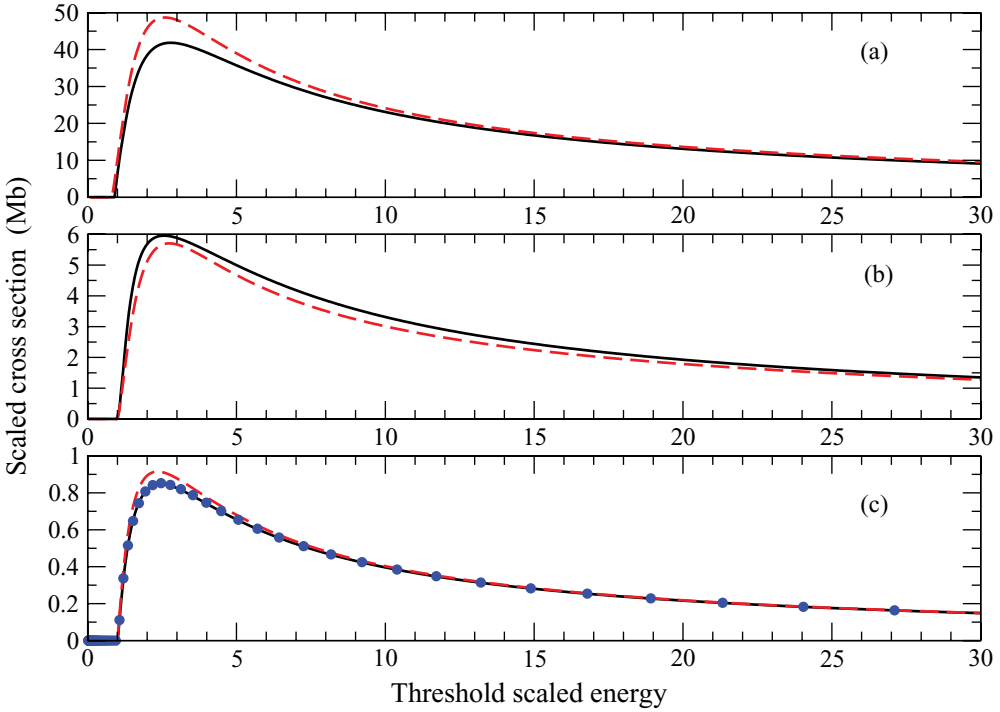

FIG. 5. (Color online) n-scaled electron-impact-ionization cross sections vs threshold scaled energy, that is, cross section divided by n^4 for the n-bundled excited states of (a) B, (b) B^+, and (c) B^{2+}. In all plots the solid line shows the $n = 3$ RMPS data, the dashed line shows the $n = 4$ RMPS data and in panel (c) the solid circles show the $n = 5$ RMPS data (1 Mb $= 10^{-18}$ cm^2).

been achieved. It may be that uncertainties in our $4d$ and $4f$ cross sections are contributing to this difference, or it may be that higher n-shell data are needed to achieve convergence. The effects of a 20% error on the excited-state ionization cross sections would carry through to less than a 20% error on the effective ionization rate coefficient. Thus, we expect that the currently calculated data for neutral B can be used with some confidence in the generation of boron GCR data.

Thus, if one bundles all of the data within an n shell, then extrapolation to higher n shells for these ions appears to be possible. The situation is a little more complicated when one looks at bundled-nS data. In this case, only the B^+ results in multiple spin systems. If we produce bundled-nS data for this ion, we get bundled-n data for the singlets and the triplets for each n shell. We find that the $n = 3$ triplets and the $n = 4$ triplets are very close to each other on an n^4 scaled plot; however, the $n = 3$ singlets are about 20% higher than the $n = 4$ singlets cross sections on an n^4 scaled cross-section plot. The reason for this is that the term splitting for the $n = 3$ shell is still significant for B^+, while the terms are almost degenerate in energy for the $n = 4$ shell. Thus, when looking at the n scaling, there are increased target correlation effects in the $n = 3$ data that breaks some of the n-scaling behavior. This is not seen in the bundled-n data because those cross sections will lie close to the triplet cross sections due to their larger statistical weight. Thus, when looking at n scaling of excited-state ionization cross sections, one should have calculations up to an n shell, where the term splitting within a configuration is negligible, and then at least one higher n shell to test convergence onto the n^4 scaling. In this case, we only have one n-shell with no significant term splitting ($n = 4$). However, the fact that the bundled-n data shows good n^4 scaling makes it seem reasonable that the bundled-nS data for $n = 4$ should be close to converged onto a similar scaling.

We fitted Eqs. (5) and (8) to the bundled-n cross sections for the highest n shell calculated in each ion. The results are shown in Fig. 6 for Eq. (8). Figure 6(a) shows the $\sum_{l=0}^{3} 1s^2 2s^2 4l$ n-bundled excited configurations for neutral B. Results using Eq. (8), matched at the peak of the $n = 4$ RMPS cross section with a fitting factor of $F^{\mathrm{bv}} = 0.46$, are also shown in Fig. 6(a). A similar fit was done with the ECIP expression [Eq. (5)] and a scaling factor of $F^{\mathrm{ecip}} = 1.62$ was obtained. Figure 6(b) shows the total cross sections for the electron-impact ionization of the $\sum_{l=0}^{3} 1s^2 2s 4l$ n-bundled excited configurations of B^+. The results using Eqs. (8) and (5), matched at the peak of the $n = 4$ RMPS cross section, gives fitting factors of $F^{\mathrm{bv}} = 1.02$ and $F^{\mathrm{ecip}} = 2.65$. Figure 6(c) shows the total cross sections for the electron-impact ionization of the $\sum_{l=0}^{4} 1s^2 5l$ n-bundled excited configurations of B^{2+}. Results using the two semiempirical equations, matched at the peak of the $n = 5$ RMPS cross section, result in fitting factors of $F^{\mathrm{bv}} = 0.76$ and $F^{\mathrm{ecip}} = 2.0$. Thus, using Eqs. (5) or (8) with the preceding scaling factors should produce accurate data for each of the ions for the higher n shells.

IV. SUMMARY

Nonperturbative close-coupling methods have been applied to calculate electron-impact-ionization cross sections for excited states of B, B^+, and B^{2+}. The RMPS and TDCC cross sections for the $1s^2 2s^2 3s$ configuration of B, the $1s^2 2s 3s$ configuration of B^+, and the $1s^2 3s$ configuration

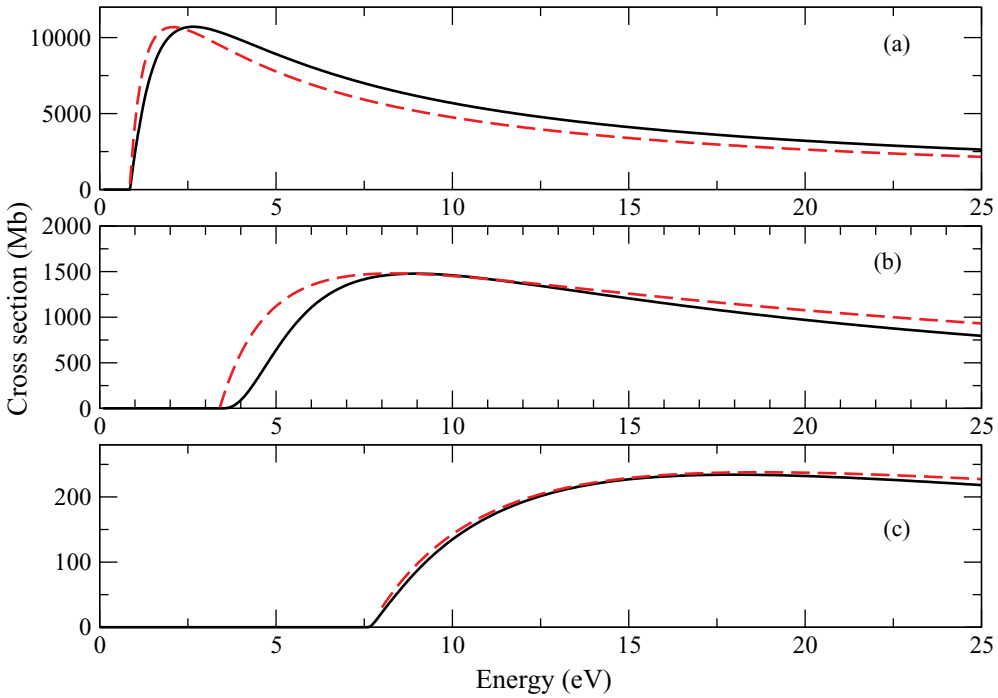

FIG. 6. (Color online) Total electron-impact-ionization cross sections for the n bundled excited states of B, B^+, and B^{2+}. (a) Solid line, B $n = 4$ RMPS; dashed line, B $n = 4$ Burgess-Vriens [Eq. (10)]. (b) Solid line, B^+ $n = 4$ RMPS; dashed line, B^+ $n = 4$ Burgess-Vriens [Eq. (10)]. (c) Solid line, B^{2+} $n = 5$ RMPS; dashed line, B^{2+} $n = 5$ Burgess-Vriens [Eq. (10)] (1 Mb $= 10^{-18}$ cm^2).

of B^{2+} were found to be in reasonable agreement. We have proposed a scheme to extrapolate the low n-shell ionization cross sections calculated using nonperturbative methods to provide ionization cross sections for higher n shells. In this scheme, as long as one has nonperturbative cross section data up to a high-enough n shell that the n^4 scaling can be demonstrated, then the results can be extrapolated to higher n shells. Thus, this method could be used for other elements to obtain high n-shell ionization cross sections. For the cases studied in this article, two semiclassical ionization cross section expressions were fitted to the peak of the RMPS n-bundled cross sections for the $\sum_{l=0}^{3} 1s^2 2s^2 4l$ configurations of B, for the $\sum_{l=0}^{3} 1s^2 2s 4l$ configurations of B^+, and for the $\sum_{l=0}^{4} 1s^2 5l$ configurations of B^{2+}. The fitted expressions will be used to help carry out generalized collisional-radiative calculations for temperature- and density-dependent ionization coefficients along the entire B isonuclear sequence. Future plans include nonperturbative close-coupling calculations for the electron-impact ionization of ground and excited states of atoms and low-charged atomic ions in the C and Ne isonuclear sequences.

ACKNOWLEDGMENTS

This work was supported in part by grants from the U.S. Department of Energy, the U.S. National Science Foundation, and the UN International Atomic Energy Agency. Computational work was carried out at the National Energy Research Scientific Computing Center in Oakland, CA, and at the National Institute for Computational Science in Oak Ridge, TN.

[1] H. P. Summers, W. J. Dickson, M. G. O'Mullane, N. R. Badnell, A. D. Whiteford, D. H. Brooks, J. Lang, S. D. Loch, and D. C. Griffin, Plasma Phys. Controlled Fusion **48**, 263 (2006).
[2] M. S. Pindzola, S. D. Loch, J. Colgan, and C. J. Fontes, Phys. Rev. A **77**, 062707 (2008).
[3] S. D. Loch, J. Colgan, M. C. Witthoeft, M. S. Pindzola, C. P. Ballance, D. M. Mitnik, D. C. Griffin, M. G. O'Mullane, N. R. Badnell, and H. P. Summers, At. Data Nucl. Data Tables **92**, 813 (2006).
[4] J. P. Allain, D. G. Whyte, and J. N. Brooks, Nucl. Fusion **44**, 655 (2004).
[5] K. Bartschat, E. T. Hudson, M. P. Scott, P. G. Burke, and V. M. Burke, J. Phys. B **29**, 115 (1996).
[6] T. W. Gorczyca and N. R. Badnell, J. Phys. B **30**, 3897 (1997).
[7] I. Bray, D. V. Fursa, A. S. Kheifets, and A. T. Stelbovics, J. Phys. B **35**, R117 (2002).
[8] C. W. McCurdy, M. Baertschy, and T. N. Rescigno, J. Phys. B **37**, R137 (2004).
[9] M. S. Pindzola *et al.*, J. Phys. B **40**, R39 (2007).
[10] D. C. Griffin, C. P. Ballance, M. S. Pindzola, F. Robicheaux, S. D. Loch, J. A. Ludlow, M. C. Witthoeft, J. Colgan, C. J. Fontes, and D. R. Schultz, J. Phys. B **38**, L199 (2005).
[11] Y. Ralchenko, R. K. Janev, T. Kato, D. V. Fursa, I. Bray, and F. J. de Heer, At. Data Nucl. Data Tables **94**, 603 (2008).
[12] I. Bray, I. McCarthy, J. Wigley, and A. T. Stelbovics, J. Phys. B **26**, L831 (1993).

[13] [http://atom.curtin.edu.au/CCC-WWW/index.html].
[14] J. C. Berengut, S. D. Loch, M. S. Pindzola, C. P. Ballance, and D. C. Griffin, Phys. Rev. A **76**, 042704 (2007).
[15] J. J. Marchalant and K. Bartschat, J. Phys. B **30**, 4373 (1997).
[16] J. C. Berengut, S. D. Loch, M. S. Pindzola, C. P. Ballance, D. C. Griffin, M. Fogle, and M. E. Bannister, Phys. Rev. A **78**, 012704 (2008).
[17] R. A. Falk, G. Stefani, R. Camilloni, G. H. Dunn, R. A. Phaneuf, D. C. Gregory, and D. H. Crandall, Phys. Rev. A **28**, 91 (1983).
[18] O. Woitke, N. Djuric, G. H. Dunn, M. E. Bannister, A. C. H. Smith, B. Wallbank, N. R. Badnell, and M. S. Pindzola, Phys. Rev. A **58**, 4512 (1998).
[19] P. J. Marchalant, K. Bartschat, and I. Bray, J. Phys. B **30**, L435 (1997).
[20] B. Lipschultz *et al.*, Phys. Plasmas **13**, 056117 (2006).
[21] K. A. Berrington, W. B. Eissner, and P. H. Norrington, Comput. Phys. Commun. **92**, 290 (1995).
[22] D. M. Mitnik, D. C. Griffin, C. P. Ballance, and N. R. Badnell, J. Phys. B **36**, 717 (2003).
[23] C. P. Ballance and D. C. Griffin, J. Phys. B **37**, 2943 (2004).
[24] L. S. Blackford *et al.*, *ScaLAPACK Users' Guide* (SIAM Publications, Philadelphia, 1997).
[25] M. S. Pindzola and F. Robicheaux, Phys. Rev. A **54**, 2142 (1996).
[26] C. Froese Fischer, Comput. Phys. Commun. **43**, 355 (1987).
[27] S. M. Younger and T. D. Mark, in *Electron Impact Ionization*, edited by T. D. Mark and G. H. Dunn (Springer-Verlag, Wien, 1985).
[28] A. Burgess, in *Atomic Collision Processes*, edited by M. R. C. McDowell (North-Holland Publ. Co., Amsterdam, 1963), p. 237.
[29] A. Burgess and H. P. Summers, Mon. Not. R. Astron. Soc. **174**, 345 (1976).
[30] See [http://vanadium.rollins.edu/GASP/GASP.html].
[31] N. R. Badnell, J. Phys. B **30**, 1 (1997).
[32] A. Burgess, M. C. Chidichimo, and J. A. Tully, J. Phys. B **30**, 33 (1997).
[33] J. M. Rost and T. Pattard, Phys. Rev. A **55**, R5 (1997).
[34] A. D. Whiteford, N. R. Badnell, C. P. Ballance, M. G. O'Mullane, H. P. Summers, and A. L. Thomas, J. Phys. B **34**, 3179 (2001).